

ERG voltage-gated K⁺ channels regulate excitability and discharge dynamics of the medial vestibular nucleus neurones

Mauro Pessia¹, Ilenio Servettini¹, Roberto Panichi¹, Leonardo Guasti², Silvarosa Grassi¹, Annarosa Arcangeli², Enzo Wanke³ and Vito Enrico Pettorossi¹

¹Department of Internal Medicine, Section of Human Physiology, University of Perugia, Via del Giochetto, I-06126 Perugia, Italy

²Department of Experimental Pathology and Oncology, University of Firenze, Viale Morgagni, 50, I-50134 Firenze, Italy

³Department of Biotechnology and Biosciences, University of Milano Bicocca, Piazza della Scienza 2, I-20126, Milano, Italy

The discharge properties of the medial vestibular nucleus neurones (MVNn) critically depend on the activity of several ion channel types. In this study we show, immunohistochemically, that the voltage-gated K⁺ channels ERG1A, ERG1B, ERG2 and ERG3 are highly expressed within the vestibular nuclei of P10 and P60 mice. The role played by these channels in the spike-generating mechanisms of the MVNn and in temporal information processing was investigated electrophysiologically from mouse brain slices, *in vitro*, by analysing the spontaneous discharge and the response to square-, ramp- and sinusoid-like intracellular DC current injections in extracellular and whole-cell patch-clamp studies. We show that more than half of the recorded MVNn were responsive to ERG channel block (WAY-123,398, E4031), displaying an increase in spontaneous activity and discharge irregularity. The response to step and ramp current injection was also modified by ERG block showing a reduction of first spike latency, enhancement of discharge rate and reduction of the slow spike-frequency adaptation process. ERG channels influence the interspike slope without affecting the spike shape. Moreover, in response to sinusoid-like current, ERG channel block caused frequency-dependent gain enhancement and phase-lead shift. Taken together, the data demonstrate that ERG channels control the excitability of MVNn, their discharge regularity and probably their resonance properties.

(Received 23 April 2008; accepted after revision 14 August 2008; first published online 21 August 2008)

Corresponding author M. Pessia: Department of Internal Medicine, Section of Human Physiology, University of Perugia, Via del Giochetto, I-06126 Perugia, Italy. Email: pessia@unipg.it

Medial vestibular nucleus neurones (MVNn) convey vestibular and visual signals from the labyrinth and peripheral retina to stabilize the eye and head and assure accurate gaze stability. Their response to peripheral activation is not only dependent on synaptic networks, but also on the dynamic properties of the neuronal membrane. Therefore, considerable efforts have been made to characterize MVNn membrane properties, ionic conductance and intrinsic excitability (for review see Straka *et al.* 2005). The aim of this research was to investigate the neurophysiological role of the ERG voltage-gated K⁺ channels in the MVNn of the mouse. Our interest in this type of K⁺ channels is based on their wide expression in many motor, sensory and integrative nuclei in the brainstem, such as the facial nucleus, cochlear nuclei, reticular nuclei and in the cerebellar Purkinje neurones

(Saganich *et al.* 2001; Papa *et al.* 2003; Polvani *et al.* 2003; Guasti *et al.* 2005), including preliminary evidence of their localization in the mouse MVN (Guasti *et al.* 2005). A particular reason for investigating the role of these channels in the MVN is also their distinct functional properties (Bauer & Schwarz, 2001; Schwarz & Bauer, 2004; Arcangeli, 2005) that are remarkably different from other K⁺ channels, including the calcium-dependent K⁺ channels BK and SK, that have been shown to shape the action potentials (APs) of type A and type B neurones and to modulate their discharge pattern (Serafin *et al.* 1991a,b; de Waele *et al.* 1993; Johnston *et al.* 1994; du Lac & Lisberger, 1995; Dutia & Johnston, 1998; Smith *et al.* 2002). In fact, the number of ERG channels in the open state increases progressively, depending on cell activity without affecting the AP shape. This has been demonstrated by delivering rectangular depolarizing pulses to cells expressing recombinant ERG channels, at different frequencies, which produced a sustained outward

This paper has online supplemental material.

current that developed progressively during the interpulse periods (Schönherr *et al.* 1999). It has been proposed that this mechanism contributes to the spike-frequency adaptation properties of neuroblastoma and cerebellar Purkinje cells (Chiesa *et al.* 1997; Sacco *et al.* 2003). Recently, it has been shown that these channels also modulate the excitability of dopaminergic (Nedergaard, 2004; Canavier *et al.* 2007) and embryonic spinal cord neurones (Furlan *et al.* 2007).

Because of this activity-dependent property, we predicted that the presence of ERG channels in the cell membrane of vestibular neurones would remarkably affect neurone responsiveness and regulate the temporal processing of vestibular signals. Here we demonstrate that ERG channels modulate electrical properties of the MVNn that are likely to play a crucial role in the temporal information processing underlying the vestibular responses to afferent signals.

Methods

Immunohistochemistry

This study was carried out by using brainstem tissue dissected from young (P10) and adult (P60) mice (C57BL/6). This procedure is in accordance with the regulations of the Italian Animal Welfare Act and was approved by the local Authority Veterinary Service, and is in accordance with the NIH Guide for the Care and Use of Laboratory Animals. Mice were transcardially perfused with saline (0.9% w/v sodium chloride) followed by paraformaldehyde (Sigma, UK, 4% w/v) in phosphate-buffered saline (PBS, 3.2 mM Na₂HPO₄, 0.5 mM KH₂PO₄, 1.3 mM KCl, 135 mM NaCl, pH 7.4) under terminal anaesthesia induced by chloral hydrate (300 mg (kg body weight)⁻¹ i.p.). Brains were removed and post-fixed overnight at 4°C in the same fixative, then soaked in 30% sucrose for cryoprotection. Brains were rapidly frozen and slices obtained with a freezing cryostat at 30 µm thickness, and collected in ice-cold PBS. Immunohistochemistry was performed as described previously (Guasti *et al.* 2005). The specificity of antibodies in recognizing ERG proteins in mouse brain sections has been described (Guasti *et al.* 2005). Images were acquired with a Leica DMR light microscope, equipped with a Leica DC200 digital camera, converted to greyscale and adjusted for brightness and contrast using Adobe Photoshop (v.6.0; Adobe Systems, San Jose, CA, USA). Each immunohistochemical experiment was repeated by using brainstem slices collected from three animals at both P10 and P60.

Tissue preparation for electrophysiological recordings

This study was carried out using brainstem tissue dissected from P20–P30 male mice (C57BL/6JO, Harlan, Italy).

Animal handling and care was in accordance with the regulations described above. Mice were decapitated under deep ether anaesthesia and the cranium opened to expose the entire brain. The brain was rapidly removed and put into ice-cold oxygenated artificial cerebrospinal fluid (ACSF) of composition (mM): NaCl, 124; KCl, 3; NaHCO₃, 26; KH₂PO₄, 1.25; MgSO₄, 2.5; CaCl₂, 2.1; glucose, 10; ascorbic acid, 2; saturated with 95% O₂ and 5% CO₂, pH ~7.4. A block of tissue containing the brainstem was cut into transverse slices (thickness 220–300 µm) with a vibratome. Slices containing the MVN were incubated in warmed (30 ± 1°C) oxygenated ACSF, transferred after 1 h to a submerged-type recording chamber (volume 500 µl) and perfused at a rate of 2 ml min⁻¹. The slice was secured by means of a nylon mesh glued to a U-shaped platinum wire that totally submerged the tissue in continuously flowing ACSF (warmed to 30 ± 1°C; pH ~7.4).

Extracellular recordings

Extracellular recordings were carried out by using 3 N sodium chloride-filled micropipettes (resistance 3 ± 1 MΩ). The APs of MVNn were recorded using an EPC9 amplifier (HEKA Elektronik), filtered at 3 kHz and acquired with a Pulse software (HEKA Elektronik). The firing rate of the MVNn was obtained by counting impulses over 1 s epochs or by computing the instantaneous firing frequency (IF), as 1 per spike interval. The regularity of firing was evaluated by determining the width (at 1/2 of amplitude) of the Gaussian curve fitting of IF distribution over a 30 s period.

Tight-seal whole-cell recording

Patch-clamp recordings were performed from MVNn under visual control by using Hamamatsu and Axioskop 2FS infrared-optics and were recorded in the whole-cell current-clamp configuration with an EPC9 amplifier (HEKA Elektronik) and stored in a Power Macintosh G4 computer. Patch glass pipettes were pulled in several stages to a tip of about 1 µm outside diameter, had a resistance of 3–4 MΩ and were filled with an intracellular solution containing (mM): potassium methylsulphate, 115; NaCl, 20; MgCl₂, 1.5; Hepes, 5; EGTA, 0.1; Na-ATP, 2; Na-GTP, 0.5; phosphocreatine, 10; pH ~7.4. All the data reported in this study were obtained using this solution. The electrode was advanced into the brain slice and a seal with the cell membrane obtained by applying negative pressure. Seal resistances were in the range of 5–10 GΩ. The membrane was ruptured by further suction. Data were acquired at 10–20 kHz, filtered at 3 kHz with a Pulse software (HEKA Elektronik) and analysed with Pulse-fit (HEKA Elektronik) and Origin7 program. Current-clamp recordings were performed in the fast speed operating

mode that allows better following of rapid changes in membrane potential, such as in neuronal action potential (www.heka.com).

Drugs

The drugs were diluted to their final concentration in ACSF and were applied by switching to a superfusion solution that differed only in its drugs content. Complete exchange of the bath solution occurred in about 2 min. In particular, the experiments were performed by perfusing the brain slices with ACSF and by adding receptor blockers (RB) for GABA_A (GABAzine, 10 μ M), AMPA (NBQX, 10 μ M), and NMDA (D-AP5, 50 μ M). The use of GABA_A and glutamate receptor blockers is necessary to avoid local spontaneously active glutamatergic and GABAergic neurones impinging on the examined neurones influencing their excitability (Dutia *et al.* 1992; Lin & Carpenter, 1993). The solution with GABA and glutamate receptor blockers (RB) was used as control condition. To block ERG channels we added WAY-123,398 (WAY) to ACSF containing RB or, in few experiments, RB plus E4031. This overall procedure was used for all electrophysiological experiments and the parameters were collected and analysed under RB and WAY, unless otherwise stated. The drugs were purchased from Tocris Cookson (Bristol, UK) and included the GABA_A receptors antagonists, (–)-bicuculline methochloride (20 μ M) and GABAzine (10 μ M, GZ), the NMDA receptor antagonist, DL-2-amino 5-phosphonopentanoic acid (AP-5, 50 μ M) and the AMPA receptor antagonist, 6-cyano-7-nitroquinoxaline-2,3-dione (NBQX, 10 μ M). To assess the functional role of ERG channels in MVNn, we used 2 μ M WAY-123,398 [(4-methylsulphonil)amido] benzenesulphonamide) which belongs to class III anti-arrhythmic agents that block all ERG channel types at this concentration, in a voltage-independent fashion (Spinelli *et al.* 1993; Masi *et al.* 2005; Faravelli *et al.* 1996). WAY-123,398 was a generous gift from Dr W. Spinelli, Wyeth-Ayerst Research, Princeton, NJ, USA. We also used 10 μ M E4031 (1-[2-(6-methyl-2-pyridyl)ethyl]-4-(4-methylsulphonylaminobenzoyl) piperidine), another blocking agent belonging to class III anti-arrhythmics (Sanguinetti & Jurkiewicz, 1990), to confirm the experimental evidence obtained by using WAY. Aliquots of stock solutions were prepared for all drugs in distilled water and stored at –20°C.

Data analysis

The firing response of the neurones was examined using step-, ramp- and sinusoid-like DC current injections through the recording electrode. Depolarizing stepwise current pulses (50–100 pA) of different durations (up to

1 s) were delivered from a holding current that maintained the neurone membrane potential at approximately –70 mV. Ramp-like current injections were applied for 3 s from a membrane potential set approximately at –70 mV up to a final steady-state value of approximately –40 mV, maintained for 3 s.

Sinusoidally modulated DC current injections were delivered at frequencies ranging from 0.5 to 10 Hz. The membrane potential was gradually set to a value that induced a firing rate ranging from 20 to 35 impulses s^{–1}. During this period all membrane conductance evoked by firing was assumed to have reached equilibrium. The basal level of injected current (typically 0.05 nA) and the amplitude of sinusoidal modulation (typically \pm 0.03 nA) were set in order to avoid firing cut-off, during the hyperpolarizing phase of current modulation, and firing saturation, during the depolarizing phase. The IF from five consecutive sweeps, composed of six oscillations at each frequency, were calculated and superimposed. The IFs of each sweep were included in the analysis only when more than four IF data points were present in a single cycle of oscillation. The sinusoidal function, $f(t) = A + B \sin(2\pi ft + C)$, was used to fit these data. The phase of the firing modulation was calculated by considering the C parameter of the formula and the gain by evaluating the ratio of Δ IF and Δ I (injected current).

The recordings were performed after \geq 10 min of stable seal formation and were analysed on condition that AP amplitudes were \geq 80 mV and the resting membrane potentials did not change more than 2–3 mV throughout the entire recording period. The AP parameters were computed using software developed in-house. In particular, the spike threshold was defined as the membrane potential at which the first derivative of the membrane potential exceeded 10 V s^{–1}. The AP height was measured from threshold to peak and AP duration by computing the interval beginning at AP threshold and ending at the point at which the horizontal line passing through the potential threshold intercepted the falling phase of the potential. The amplitude of the AHP was measured as the amplitude difference between the threshold and the minimal membrane potential in type A neurones and between the threshold and the minimal potential of the fast component of AHP (AHP_f) in type B neurones. The afterdepolarization potential (ADP) of type B neurones was measured from the peak of the AHP_f and the first upward oscillation. The steepness of the potential variation between adjacent APs (named interspike slope steepness) was evaluated by calculating the mean derivative of the straight line intercepting both the AHP_f in type B neurones (or the AHP in type A) and the AP threshold of the next spike. Input resistance (R_{in}) was computed by injecting hyperpolarizing currents (typically 10 pA) and measuring the membrane potential

deflection. The IF was computed by measuring the interval between spikes, and the time at the end of each interval was used to indicate the time for each IF. First spike latency was calculated as the time elapsing from the stimulus onset to the first AP threshold. The steepness of IF enhancement, elicited by the ramp, was expressed as the angular coefficient of the linear regression fitting of the relevant values. The time course of the progressive IF variation, observed in most neurones during both ramp and steady phase of current injection, was evaluated by fitting the IF data points with the exponential function, $y = A1 \cdot \exp(-x/t1) + y0$, from which the rise (τ_r) and decay time (τ_d) constants were calculated.

Different cell types have been found in the vestibular nuclei, spanning a continuum of electrophysiological properties, with different functional properties namely related with the tonic and dynamic responsiveness of neurones. The classification of type A (tonic) and B (phasic-tonic) neurones was performed by considering AP width (type A, 0.6–1 ms; type B, 0.4–0.6 ms) AP half-width (type A, 0.26–0.46 ms; type B, 0.14–0.24 ms), AHP amplitude (type A, 25–30 mV; type B, 15–25 mV) and the presence of ADP (Fig. 3; Serafin *et al.* 1991a,b; Johnston *et al.* 1994; Babalian *et al.* 1997; Takazawa *et al.* 2004; Straka *et al.* 2005; Bagnall *et al.* 2007). In addition, we plotted the maximum value of the spike derivative during the 1 ms after the spike repolarized to threshold level (V/s of ADP) *versus* spike half-width, as a criterion to distinguish GABAergic from non-GABAergic neurones (Bagnall *et al.* 2007). In our study, RNs and UNs were found scattered among both type A and B neurones and both GABAergic and non-GABAergic neurones.

Statistical evaluation

The statistical significance of the differences observed before and after WAY application in the neuronal discharge was performed in each experiment for all parameters (firing, interspike slope, latency, τ_r and τ_d) using repeated measures ANOVA and Tukey's *post hoc* test. The difference was considered significant at $P < 0.05$. Neurones showing significant changes in firing rate were named responsive neurones (RNs) and those that did not were named unresponsive neurones (UNs). Student's *t* tests were also performed to compare the global effects on RNs *versus* UNs, shown in Figs 2, 4, 6 and 7. The goodness of the fit was estimated by calculating the χ^2 for sine function and by correlation coefficient (*R*) for linear and first order decay exponential function. The best fit was obtained by minimizing the mean square error between the data and the curve (Levenberg–Marquardt algorithm). The goodness of fit was regressed against actual firing rate values with regression lines always close to 1 and R^2 between 0.95 and 0.90).

Results

Immunohistochemical localization of ERG channels within murine vestibular nuclei

Several members of functionally distinct classes of voltage-gated K^+ channels have been cloned and classified into different subfamilies, including the EAG (ether-à-go-go), ELK (eag-like K^+ channel) and ERG (eag-related; Kv11). To date, four ERG channels have been cloned and named ERG1A, ERG1B, ERG2 and ERG3 (Warmke & Ganetzky, 1994; Shi *et al.* 1997; London *et al.* 1997; Lees-Miller *et al.* 1997). In order to determine the localization of ERG channel types within the vestibular nuclei, rabbit polyclonal anti-ERG1A, anti-ERG1B, anti-ERG2 and anti-ERG3 antibodies were produced, purified and tested as previously described (Cherubini *et al.* 2000; Guasti *et al.* 2005). By using these antibodies, a positive immunoreactivity was observed within the brainstem slices dissected from P60 C57/BL mice. Many, but not all, cells located within the medial, superior, lateral and descending vestibular nuclei were immunopositive for ERG1A, ERG1B, ERG2 and ERG3 proteins (Fig. 1A–E). In particular, the high magnification images of Fig. 1 show numerous neurones, within the MVN, stained with all the antibodies. As reported for other brain regions (Guasti *et al.* 2005), ERG2 appeared to be the least expressed amongst the channel subfamily. To examine the expression of these channel proteins, also at a younger stage of development, brainstem slices containing the vestibular nuclei were dissected from P10 mice. A significant labelling for all ERG channel types was also detected within the vestibular nuclei of these specimens. Indeed, the expression patterns of ERG channels in brainstem slices dissected from P10 and P60 mice were very similar (Fig. 1F–I). At both ages, the antibodies showed a preferential staining for the soma of vestibular neurones. Moreover, cells not stained or weakly stained (white arrows) could be detected amongst positively labelled cells (black arrows). The results obtained from three independent experiments were substantially similar and no relevant differences were detected between the two ages. These observations demonstrated that several ERG channel types are expressed by vestibular neurones. It is likely that the channels are expressed during the early period of postnatal development as well as during the adulthood of mammalian species.

ERG channel modulation of the spontaneous activity of MVNn

We recorded 17 MVNn extracellularly, under RB (control condition) and WAY to analyse the effect of ERG channel block on the spontaneous discharge of these neurones in the absence of main glutamatergic and GABAergic inputs

(Fig. 2C). A significant enhancement of the spontaneous firing rate was seen in 10 out of 17 neurones after WAY from 19.5 ± 4.7 to 24.6 ± 4.5 spikes s^{-1} ($P < 0.001$) (Fig. 2A and F). These were named responsive neurones (RNs). Conversely, the remaining 7 unresponsive neurones (UNs) showed no significant changes in their spontaneous discharge rates ($P > 0.05$; Fig. 2B and F). The firing frequency of RNs increased shortly after WAY infusion, and slowly reached a steady-state value 20 min later. This effect reversed very slowly after drug washout and usually lasted for all the recording period (more than 60 min). RNs also displayed a significant increase in discharge irregularity after WAY infusion that can be evinced by the enlargement of the Gaussian width, from 1.53 ± 0.2 (RB) to 2.38 ± 1.0 (WAY) (Fig. 2D and G; $P < 0.01$). The neurone firing irregularity consisted of frequency fluctuations with unpredictable intervals in the order of seconds or minutes. No significant width changes were observed in UNs upon ERG channel blockade (RB: 1.56 ± 0.6 ; WAY: 1.31 ± 0.8 ; ($P > 0.05$, Fig. 2E and G).

ERG channel modulation of MVNn discharge in response to square-like DC current injection

The electrophysiological properties of MVNn modulated by ERG channels were also analysed by means of whole-cell patch-clamp recordings, in current-clamp mode, before (RB) and after channel blockade (WAY). Figure 3 shows the location of RNs and UNs recorded in the MVN that were included in the analysis. Based on the AP shape, duration and discharge pattern, we classified 17 out of 20 neurones as type B (non-GABAergic) and 3 as type

A (GABAergic; Fig. 3). To evoke cell firing, square-like depolarizing current pulses (50–100 pA) were applied through the recording electrode ($E_m = \sim -70$ mV; Fig. 4). In response to a step, firing showed a first spike latency of 45–120 ms and an immediate peak of firing (IF_{peak}) of 15–90 impulses s^{-1} (Fig. 4A, D and E). Thereafter, the IF decayed to steady-state values (IF_{ss}) ranging from 10 to 40 impulses s^{-1} , exponentially, with τ_d ranging from 0.031 to 0.481 s (Fig. 4D and E). These responses were examined before (RB) and after the application of WAY. Under WAY, 70% of neurones (14 out of 20; type B, non-GABAergic, 13; type A, GABAergic, 1) showed a significant increase of their IF (RNs). In particular, both the IF_{peak} and IF_{ss} of these RNs were significantly increased by $14.5 \pm 8.9\%$ and $12.3 \pm 8.7\%$, respectively ($P < 0.001$) (Fig. 4D, F and G). The remaining UNs (type B, 4; type A, 2) did not show any significant IF change upon WAY superfusion ($P > 0.05$; Fig. 4E–G). All RNs showed a significant reduction of first spike latency of $\sim 10\%$ ($P < 0.01$; Fig. 4A and H) and an increase of steepness of interspike slope by $\sim 14\%$ at the response peak and by $\sim 12\%$ at the steady state ($P < 0.001$) (Fig. 4B, I and J). Conversely, spike threshold, amplitude, width and AHP_f were not altered, as the APs recorded before and after WAY perfectly superimposed throughout the entire stimulation period (Fig. 4C). Moreover, $\sim 30\%$ increase in the τ_d of spike frequency was observed in 10 out of 14 RNs ($P < 0.05$; Fig. 4D and K). The input resistance (R_{in}) of RNs slightly increased after ERG channel blockade (RB: 204 ± 20 M Ω ; WAY: 217 ± 26 M Ω ; $P > 0.05$). As far as UNs are concerned, we did not find any significant change under WAY in R_{in} , AP shape, frequency, latency, interspike slopes and τ_d ($P > 0.05$; Fig. 4E–K). The comparison of the AP parameters between type A (GABAergic) and type B

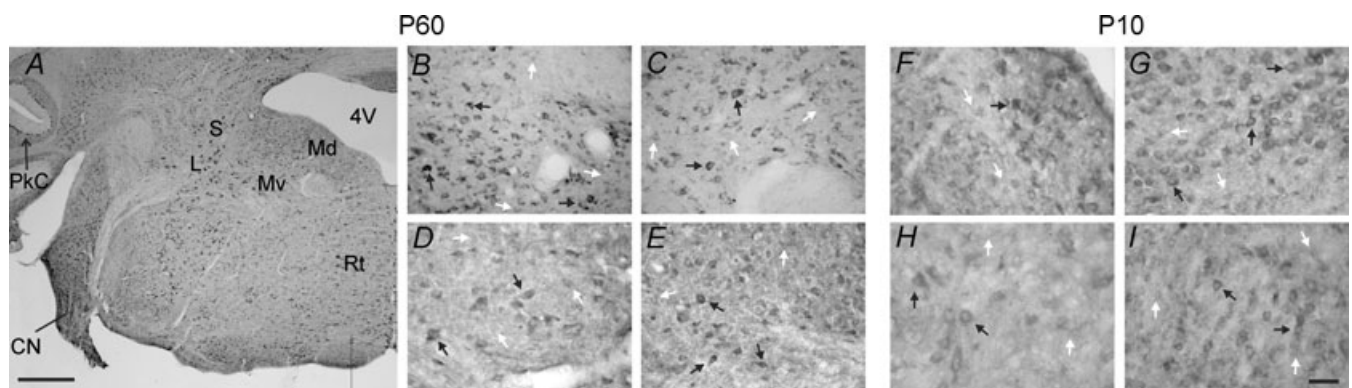
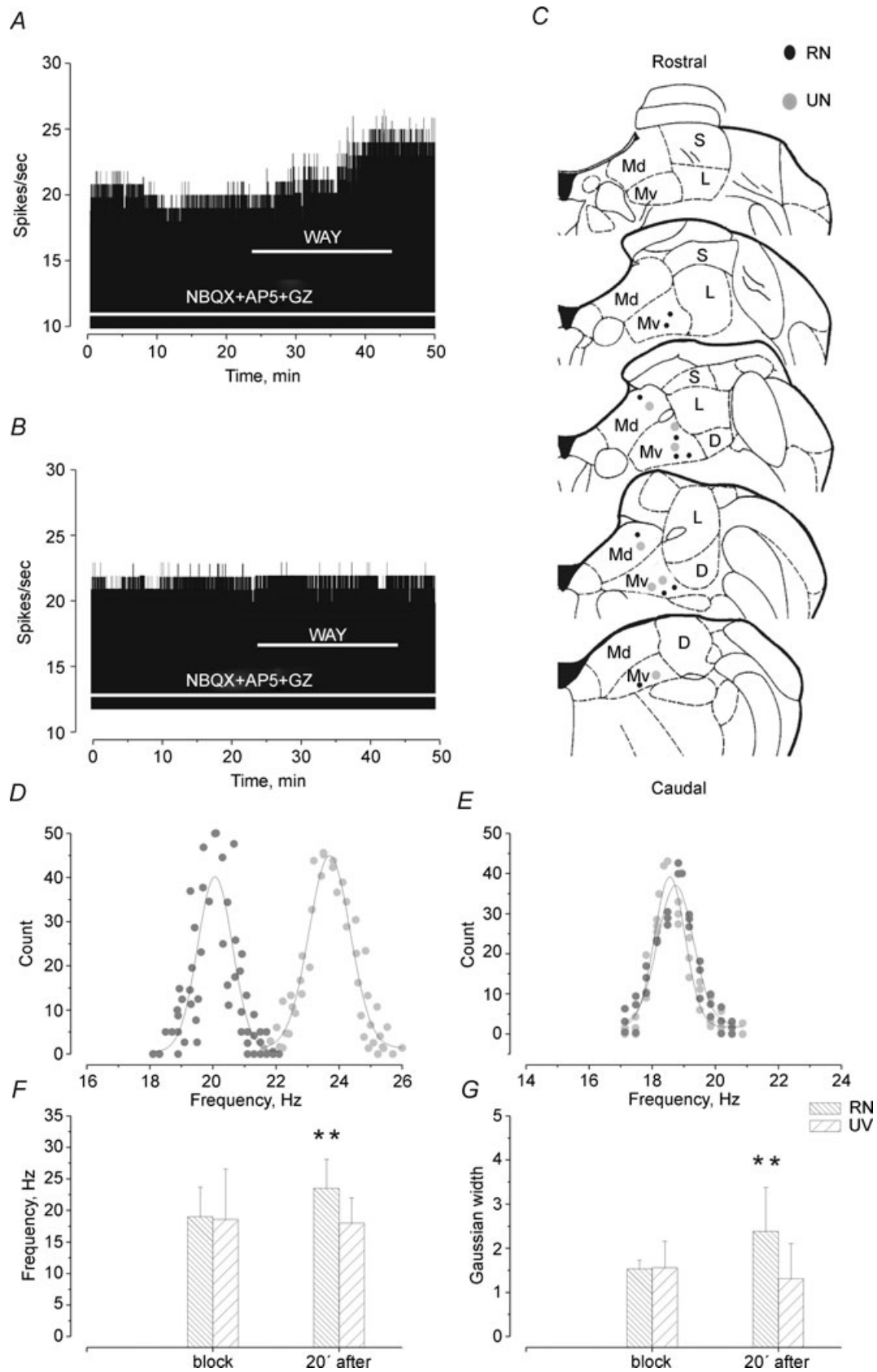


Figure 1. Immunohistochemical localization of ERG channels in the brainstem of P60 (A–E) and P10 (F–I) mice

A, low magnification image at the level of the vestibular nuclei stained with anti-ERG1B antibody. B–I, higher magnification images of MVN. B and F, anti-ERG1A; C and G, anti-ERG1B; D and H, anti-ERG2; E and I, anti-ERG3. Heavily stained cells, detected with the antibodies, are pointed out by black arrows, and weakly or unlabelled cells by white arrows. Scale bars, 250 μm in A, 25 μm in I (applies to B–H). Abbreviations: Md, medial vestibular nucleus, dorsal part; Mv, medial vestibular nucleus, ventral part; L, lateral vestibular nucleus; S, superior vestibular nucleus; 4V, fourth ventricle; CN, cochlear nucleus; PkC, cerebellar Purkinje cells; Rt, reticular nucleus.



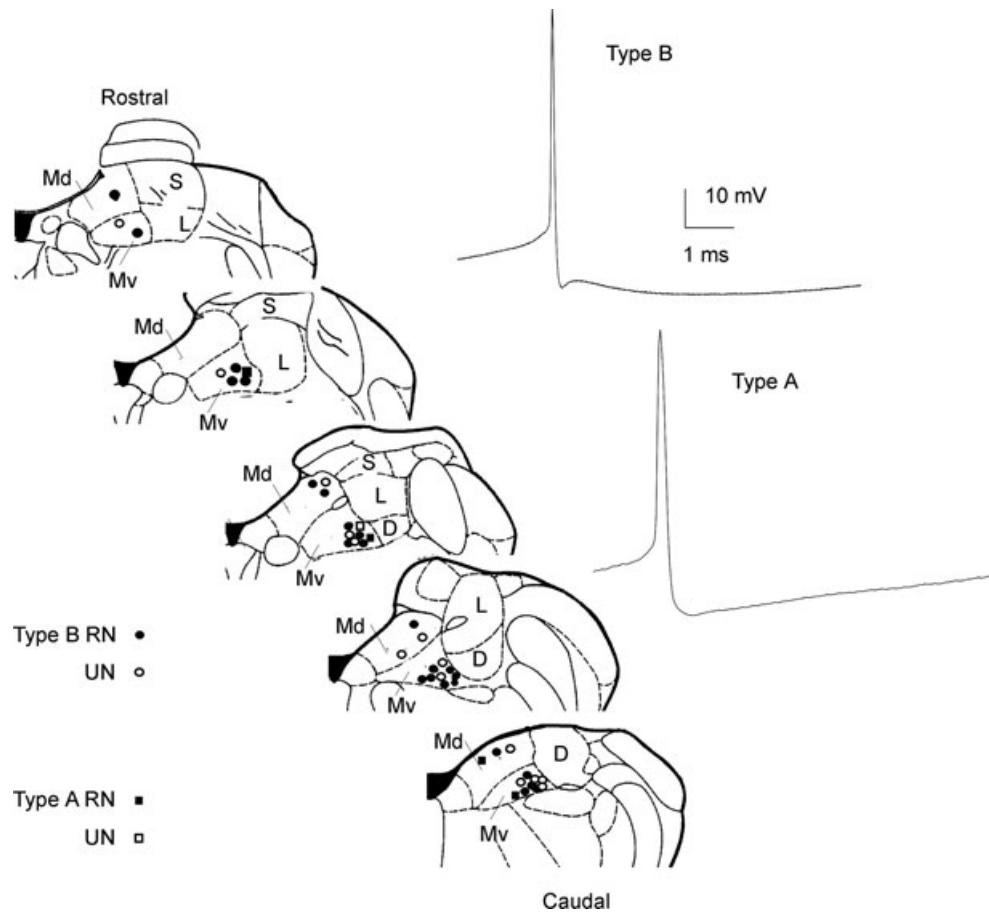


Figure 3. Whole-cell patch-clamp recordings of MVNn

Sites of type A (squares) and type B (circles) recorded within the MVN for step, ramp and sine current injections. Filled symbols indicate RNs and open symbols UNs. Neurons underwent combined or separate stimulations. Abbreviations, as in Fig. 2C. On the right, APs of type B (top) and type A (bottom) neurones.

(non-GABAergic) neurones did not show any qualitative difference, but the small sample size of type A neurones did not allow statistical evaluation. With regard to the regularity of the discharge, after WAY an increase of the IF irregularity was observed in few neurones with minimal increase of the Gaussian width (data not shown).

ERG channel modulation of MVNn discharge in response to ramp-like DC current injection

The discharge dynamic of 34 MVNn was also studied by injecting ramp-like currents intracellularly that depolarized the membrane potential from ~ -70 mV to ~ -40 mV, and was maintained steady for 3 s (Fig. 5).

Figure 2. Effect of ERG channel blockade on the spontaneous firing activity of MVNn

Rate histograms of a representative discharge pattern of: A, MVN responsive neurone (RN) and B, MVN unresponsive neurone (UN), recorded extracellularly during the superfusion of NBQX + AP-5 + GZ and of WAY (horizontal bars) into the recording chamber. The discharge frequencies were integrated over 1 s epochs. In C, the recording sites of RNs (black circles) and UNs (open circles) within the MVN are shown. Abbreviations: Md, medial vestibular nucleus, dorsal part; Mv, medial vestibular nucleus, ventral part; S, superior vestibular nucleus, L, lateral vestibular nucleus; D, descending vestibular nucleus. In D and E, histograms of firing frequency distribution of a RN (D) and an UN (E) constructed by analysing the instantaneous firing frequencies in 30 s epochs under RB (dark grey) and 20 min after WAY application (light grey). Continuous lines indicate the fitting of data points by Gaussian functions. Note the increase of both the mean and width of firing frequency distribution under WAY in RN. In F and G, bar graphs showing the mean and s.d. of firing frequency (F) and width (G) calculated from the Gaussian curve under RB and 20 min after WAY application in RNs ($n = 10$) and UNs ($n = 7$). **Student's t test $P < 0.01$.

Thirty neurones were of type B (non-GABAergic) with only four of type A (GABAergic; Fig. 3). Neurones began to discharge at potentials ranging between -51 mV and -45 mV (firing threshold) with a latency of 0.45 – 2.1 s after the beginning of current injection (Fig. 5). The time course of IF enhancement was well described by both single exponential function ($\tau_r = 0.5$ – 3.8 s) and regression line angular coefficient ranging from 4.7 to 21 . At the end of the ramp stimuli, neurones reached IF_{peak} ranging from 20 to 75 impulses s^{-1} . Afterwards, during current holding, discharge frequency decreased exponentially in most of the neurones with τ_d of 0.6 – 3.5 s and reached IF_{ss} of 15 – 50 impulses s^{-1} at the end of the holding phase

(spike frequency adaptation). Upon WAY superfusion, 21 (RNs) out of 34 neurones (type A, GABAergic, 3 ; type B, non-GABAergic, 18) showed significant increase of the IF_{peak} and IF_{ss} of $\sim 19\%$ and $\sim 39\%$, respectively ($P < 0.001$; Figs 5A–C and 6A and B). The interspike slope steepness calculated at the IF_{peak} and at the IF_{ss} increased by $\sim 22\%$ and $\sim 42\%$, respectively ($P < 0.001$; Figs 5E and 6C and D). Interestingly, the time course of the interspike slope steepness was very similar to that of IF throughout the entire ramp (Fig. 5C–F). In the remaining 13 neurones (UNs), the overall firing responses to ramp-like stimuli were unchanged ($P > 0.05$; Figs 5D and F, and 6A and B). All RNs showed a significant

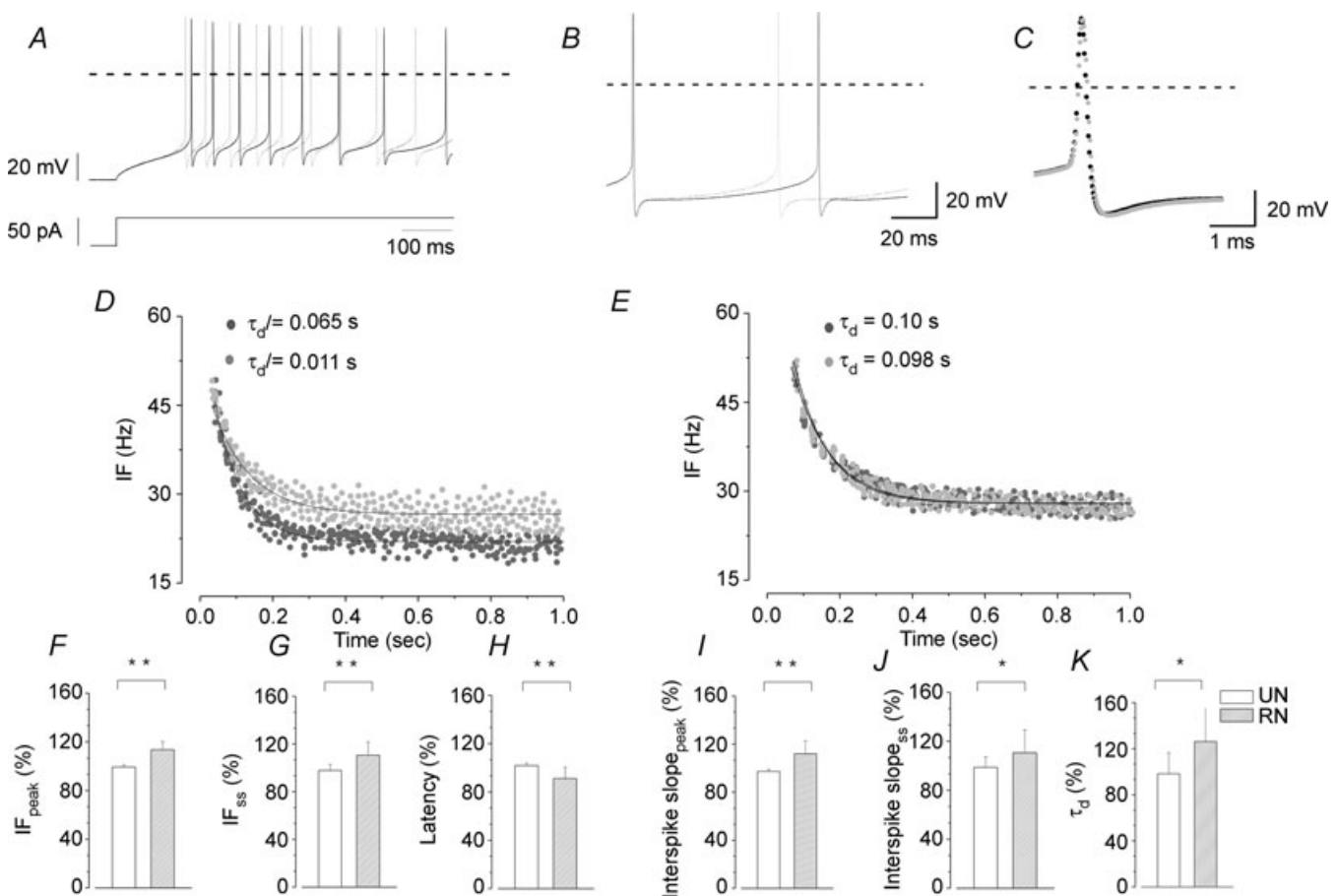


Figure 4. Response of MVNn to step-like DC current injection upon ERG channel blockade

In A, B and C, superimposition of RN responses under RB (continuous trace) and under WAY (dotted trace) evoked by 50 pA step current injection at different time scales. WAY induces shortening of the first spike latency and firing rate increase (A), increase of interspike slope steepness (B) and no changes in the AP shape (C). Note that WAY did not affect the AP amplitude, AHP duration or threshold. The horizontal dashed lines indicate the zero membrane potential. In D and E, data points are the IF of representative RN (D) and UN (E) evoked by 50 pA step stimulation before (dark grey) and under WAY (light grey). Points are fitted by exponential decay curves, from which the τ_d were calculated (values on the top). Note the τ_d increases under WAY in RN with no change in UN. In F–K, bar graphs of IF_{peak} and IF_{ss} , first spike latency, interspike slope_{peak}, interspike slope_{ss}, and τ_d . All the values are expressed as a mean \pm s.d. of percentage variation observed before and after WAY. RNs (hatched columns, $n = 17$) and UNs (open columns, $n = 6$) were grouped on the basis of frequency increase observed under WAY (F and G). Statistical comparisons were performed in H–K by Student's *t* test * $P < 0.05$, ** $P < 0.01$.

decrease in the discharge latency ($P < 0.005$) of $\sim 36\%$ (Figs 5C and 6E) and an $\sim 55\%$ increase of regression line angular coefficient that fits the enhancement of firing (data not shown). The τ_r of IF and interspike slope steepness (when exponential decay was present) increased by $\sim 70\%$ and by $\sim 80\%$, respectively (Fig. 6F and G). The τ_d of IF and interspike slope steepness increased by $\sim 88\%$ and by $\sim 92\%$, respectively ($P < 0.01$; Fig. 6H and I). Concerning the regularity of the discharge, a slight increase of the Gaussian curve width was observed in few cases after ERG channel block (data not shown). Conversely, significant changes were not observed in UNs (Fig. 6A–I). Regarding the shape of the spike, we did not find any change in either RNs or UNs, as the spikes before and after WAY perfectly superimposed both at the beginning and at the end of the ramp. Even a quantitative comparison of the AP parameters, under RB and WAY, yielded changes that were not significant (data not shown). Furthermore, WAY induced similar effects on both RN type A (GABAergic) and RN type B neurones (non-GABAergic); however,

due to the small sample size of type A neurones a quantitative comparison could not be made (data not shown).

ERG channel modulation of MVNn discharge in response to sinusoid-like DC current injection

The firing response dynamic of 21 MVNn (type A, GABAergic, 3; type B, non-GABAergic, 18) was studied by delivering sinusoid-like DC current injection (stimuli amplitude 10–30 pA; frequency range 0.5–10 Hz; Fig. 7). These sinewaves were preceded by a ramp and a steady current injection (similar to that used above), during which all membrane conductance, evoked by firing, was assumed to have reached equilibrium gradually. The basal level of injected current (typically 0.05 nA) and its amplitude (typically ± 0.03 nA) were chosen in order to increase IF to ~ 30 impulses s^{-1} , to avoid firing cut-off and saturation. The IF was faithfully modulated by the sinewave-like current (Fig. 7A and B). The phase was

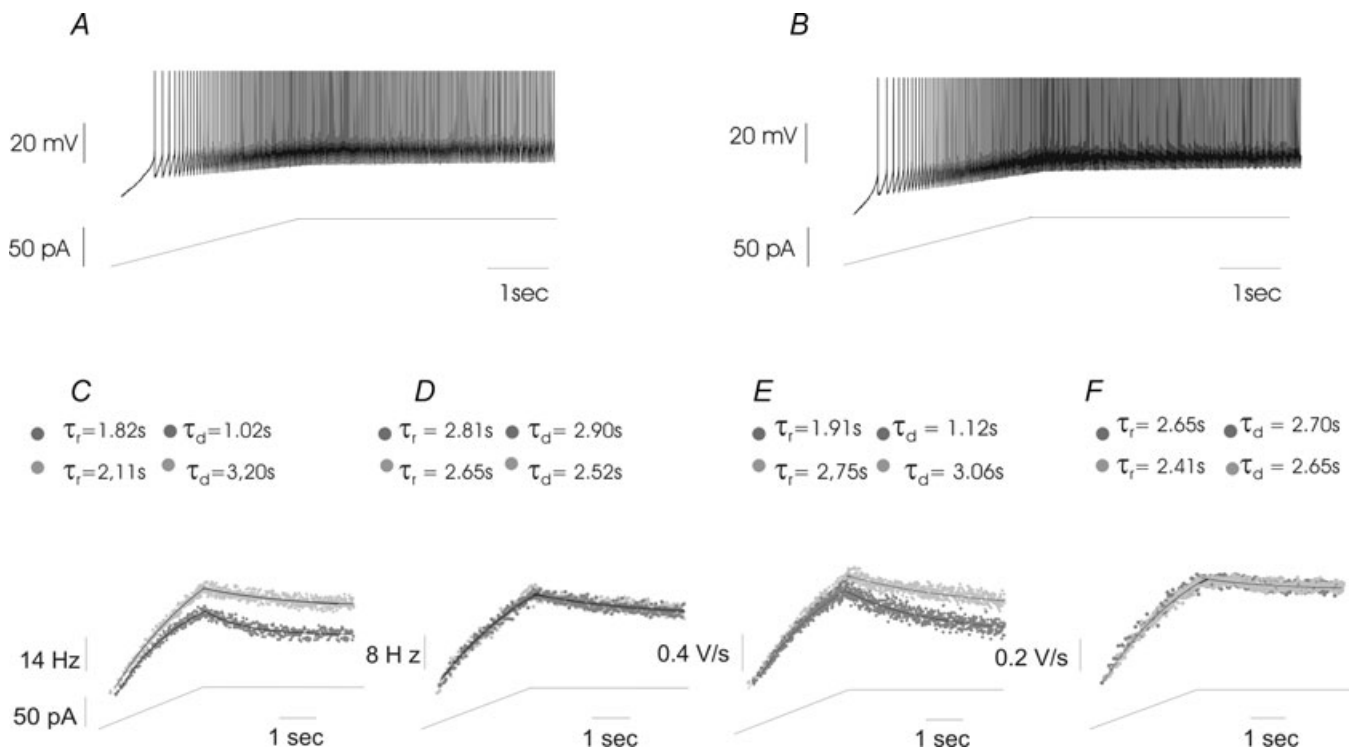


Figure 5. Response of representative MVNn to ramp-like DC current injection upon ERG channel blockade

In A and B, representative discharge pattern (upper trace) evoked by a ramp injected current (lower trace) under RB (A) and WAY (B). APs were truncated at 0 mV for clarity. In C and D and in E and F data points represent IF and interspike slope steepness, respectively, of a RN (C and E) and UN (D and F), under RB (dark grey circles) and WAY (light grey circles). The profile of the firing frequency increase and decrease of these sample neurones were best fitted by exponential functions (continuous line) to evaluate the rise (τ_r) and decay (τ_d) time constants (values at the top, dark grey, RB; light grey, WAY). Note the increase of τ_r and τ_d of IF and interspike slope steepness under WAY in RN only.

~ 5 deg lead at 0.5 Hz and gradually decreased toward lag (~ 15 deg lag) at 10 Hz (Fig. 7C). The gain, expressed as the percentage variation compared to the baseline gain at 0.5 Hz in RB condition, increased by $\sim 25\%$ from 1 to 10 Hz (Fig. 7D). Fifteen out of 21 neurones were significantly ($P < 0.0001$) influenced by WAY (type A, GABAergic, 3; type B, non-GABAergic, 12), as shown by the baseline frequency increase. Indeed, upon WAY application the firing dynamics changed in 10 out of 15 RNs (type A, GABAergic, 2; type B, non-GABAergic, 8). This change consisted of a significant phase shift toward lead of ~ 20 deg at 3, 5 and 10 Hz ($P < 0.01$; Fig. 7A–C). The gain also increased in the higher frequency range by ~ 20 – 40% ($P < 0.01$; Fig. 7D). Qualitative differences between type B (non-GABAergic) and type A (GABAergic) neurones were not observed, but again, quantitative evaluations could not be performed. The gain and phase of UNs did not show any significant change after WAY ($P > 0.05$; Fig. 7C, D).

Effect of basal discharge frequency on the response to sinusoidal current injection

In a separate group of experiments we tested the effect of different basal levels of membrane potential depolarization of the neurones during sinusoidal current injection, leading to different discharge frequencies that ranged from 25 to 45 impulses s^{-1} . Seven neurones out of 12 were RNs ($P < 0.0001$) and showed phase lead and gain increase after WAY application. In 4 out of 7 RNs neurones WAY caused a phase lead increase of 16 ± 5 deg ($P < 0.001$) in response to 3 Hz oscillations at basal frequency of 22–25 impulses s^{-1} . This phase shift decreased to 9 ± 5 deg ($P < 0.05$) at frequency of 30–33 impulses s^{-1} and it was almost null at 40–45 impulses s^{-1} ($P > 0.05$). However, this effect of basal firing frequency on phase and gain was much less evident in the other three RNs. No differences in firing rate, phase and gain were observed at different basal discharge

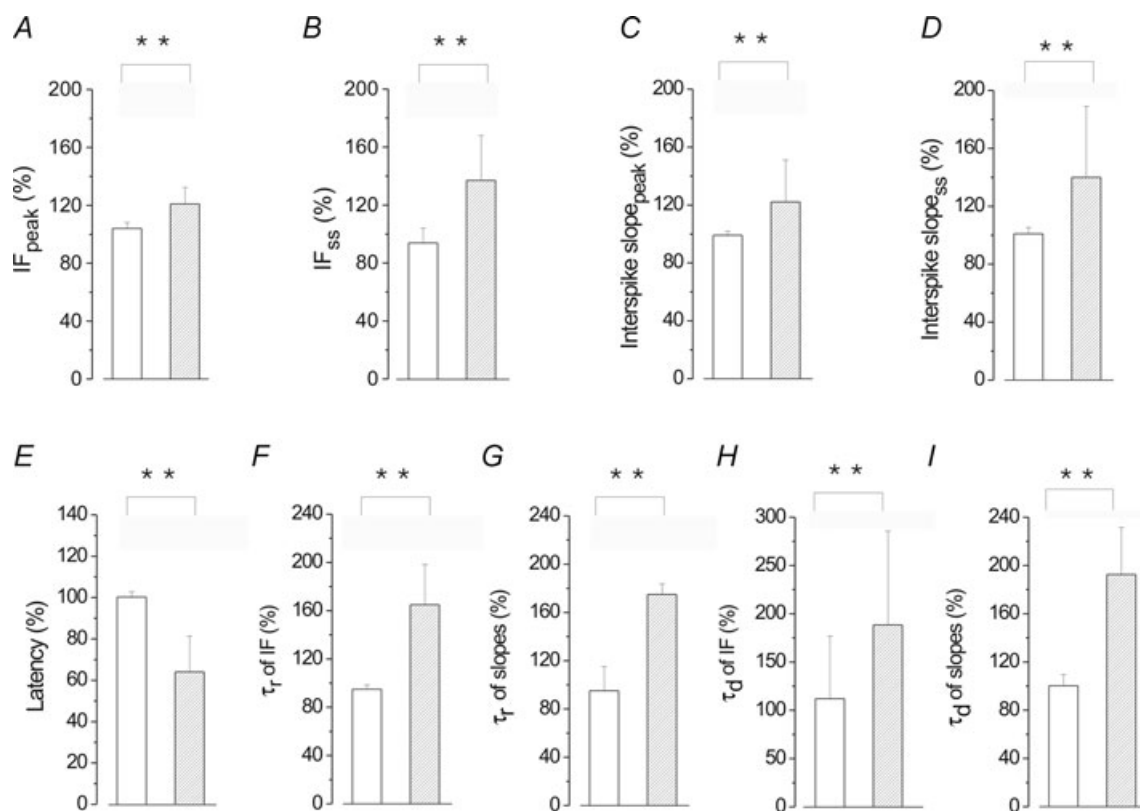


Figure 6. Evaluation of the effects of ERG channel block on the whole sample of MVNn following ramp-like DC current injection

Bar graphs showing the effects of WAY on the IF peak (A), IF_{ss} (B), interspike slope_{peak} steepness (C) and interspike slope_{ss} steepness (D), spike latency (E), τ_r of IF (F) and τ_r of interspike slope steepness (G), τ_d of IF (H) and τ_d of interspike slope steepness (I). All values are expressed as a mean \pm s.d. of percentage variation observed before and after WAY. RNs (hatched columns, $n = 21$) and UNs (open columns, $n = 13$) were grouped on the base of the WAY-dependent frequency increase, reported in A and B. Statistical comparisons were performed between these two groups, in C–I, by Student's t test * $P < 0.05$, ** $P < 0.01$.

frequencies in UNs ($P > 0.05$). These results suggest that ERG channels contribute to controlling the phase of the responses of at least some MVNn mainly at lower discharge frequencies.

Effect of the ERG channel blocker E4031 on square-, ramp- and sinusoid-like DC current injection

Additional supportive evidence for the role of ERG channels on the excitability of MVNn has been provided by using E4031, another highly specific ERG channel

blocker (Sanguinetti & Jurkiewicz, 1990). We found that with E4031 ($10 \mu\text{M}$) 4 out of 7 neurones showed $\sim 15\%$ increase of IF elicited by square-like stimulation (see Supplementary Fig. 1SA; $P < 0.001$), $\sim 10\%$ decrease of latency (Fig. 1SA; $P < 0.01$), $\sim 30\%$ τ_d increase (Fig. 1SB; $P < 0.05$). In response to ramp-like stimulation MVNn showed $\sim 28\%$ increase of IF_{peak} (Fig. 1SC; $P < 0.01$), 21% decrease of latency (Fig. 1SC; $P < 0.05$) and $\sim 75\%$ τ_d increase (Fig. 1SC; $P < 0.01$). In response to sine wave stimulation, a phase-lead shift of ~ 15 deg and gain increase of $\sim 20\%$ were observed at 3 Hz (Fig. 1SD; $P < 0.01$). Taken together these results were substantially

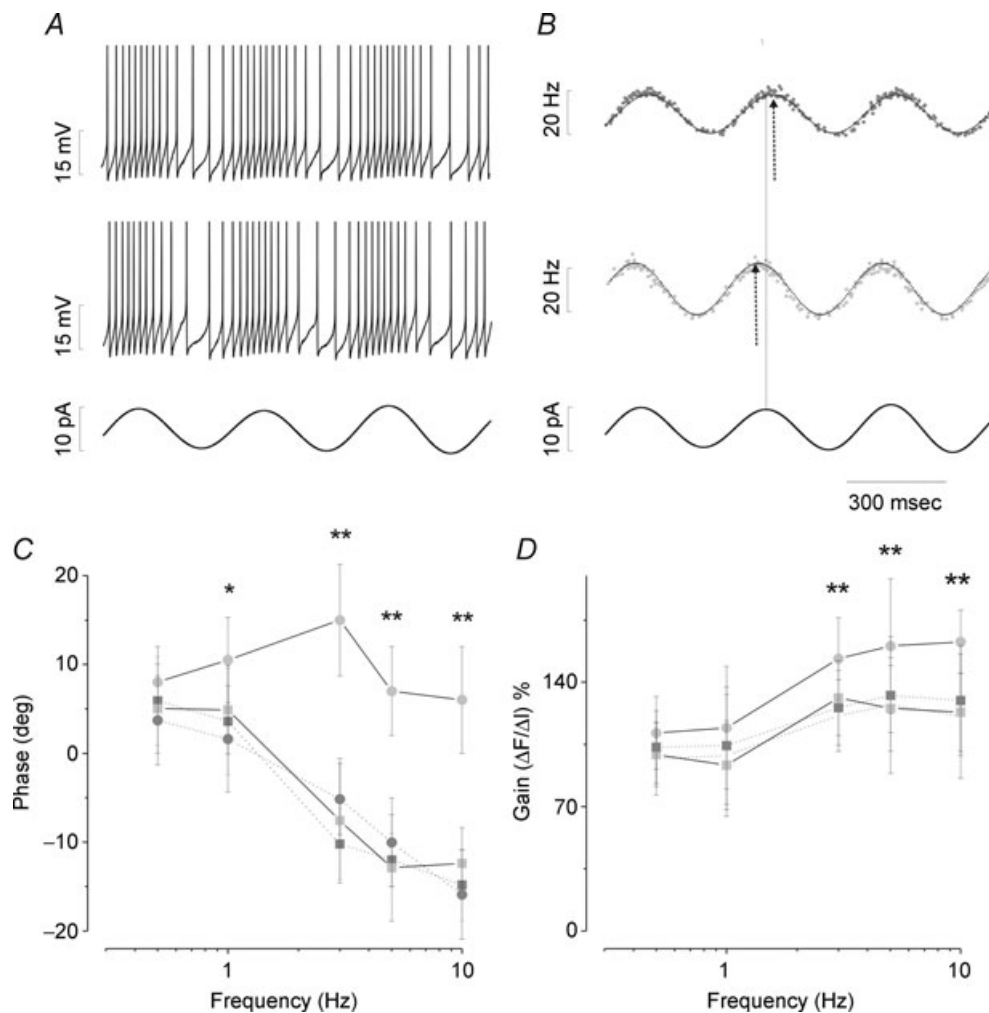


Figure 7. ERG channels modulate the gain and phase of the MVNn response to sinewave stimulation

In A, firing response of a MVNn to sinusoidal current injection under RB (upper trace) and WAY (middle trace). The intracellular current injection at 3 Hz (bottom trace) evoked a faithful sinusoidal frequency modulation. In B, IF of a MVNn under RB (upper trace) and WAY (middle trace) in response to sinusoidal current injection (bottom trace). Data points were fitted by sinusoidal curve (continuous line). The vertical line indicates the position peak of sinusoidal stimulus and the arrows the peak of IF. In C and D, bode plot of the response of neurones to sinusoidal current injection. Ten neurones (dark grey circle under RB, light grey circle under WAY) showed phase-lead shift and gain increase, whereas other 11 neurones (dark grey square under RB, light grey square under WAY) were not affected. Gain is normalized at the 0.5 Hz level under RB condition. All the values are expressed as mean \pm s.d. and significance was calculated using Student's *t* test * $P < 0.05$, ** $P < 0.01$. Note the significant phase-lead shift in the range of 1–10 Hz and a significant gain increase, particularly at higher frequencies.

similar to those obtained under WAY-123,398.

Discussion

In this study we have shown that several ERG channel types are expressed within the vestibular nuclei and modulate the discharge dynamics of MVNn.

Our immunohistochemical analysis clearly demonstrated that neurones located within the medial, superior, lateral and descending vestibular nuclei express ERG1A, ERG1B, ERG2 and ERG3 subunits. Positive labelling was observed in brainstem slices of both P10 and P60 mice for all ERG channel types, demonstrating their expression in both young and adult animals. These results, together with the electrophysiological findings, strongly suggest that these channels are present on the plasma membrane of MVNn. However, the expression levels of the different ERG subunits are unequal (e.g. ERG2 is the least expressed), suggesting that the subunit composition of the tetrameric channel may vary amongst MVNn.

Functional investigations demonstrated that ERG channel blockade induced an increase of spontaneous discharge in more than half of the cells examined in the extracellular mode. It is likely that this is a result of a direct action of the drug on the same neurone under investigation, since the main synaptic inputs from local circuits were blocked.

Because of the effect of ERG channel block on the spontaneous activity of MVNn, we conclude that ERG channels are partially opened during their basal pacemaker-like firing, contributing to setting the neurone discharge frequency. Moreover, the spontaneous discharge became less regular after channel block, suggesting that these channels are also partially involved in controlling discharge regularity. Since ERG channel opening depends on discharge frequency, any spontaneous membrane potential oscillation, responsible for frequency irregularity, would be attenuated by varying ERG channel opening. However, the effect on discharge regularity should also greatly depend on the biophysical properties of ERG channels and on the characteristics of membrane potential fluctuations. In order to investigate the mechanisms underlying the effect of ERG channel block, step, ramp and sinewave stimuli were delivered intracellularly through the patch-clamp electrode. We found that ERG channel block by both WAY and E4031 significantly increased the firing frequency of most of the neurons in response to all these stimuli, confirming the enhancement of cell excitability observed in the extracellular study. However, the increase in the discharge irregularity was only occasionally observed, probably due to different recording conditions in which the current

injections might influence the spontaneous discharge fluctuations.

The analysis of several AP parameters revealed that ERG channel block does not modify the threshold, amplitude, AHP_f, ADP and the overall shape of the spike, whereas it increases only the steepness of the interspike slopes, even after prolonged depolarization. Indeed, the time courses of the IF and interspike slopes, in response to ramp stimulation, were rather similar. Thus, we could state that the control of the discharge rates by ERG channels is basically due to an inhibitory drive on the pacemaker activity by a certain amount of outward ERG current that slows down the potential rising during the interspike periods. The removal of such a drive would increase the spontaneous firing rate as also shown by the extracellular recordings.

As far as the dynamics of ERG channel opening is concerned, it has been proposed that, during a train of APs, these channels progressively accumulate in the open state, due to their slow kinetics of deactivation. Indeed, rectangular depolarizing pulses, delivered at several frequencies to cell-lines or *Xenopus* oocytes expressing ERG channels, produce a sustained outward current that develops progressively during the interpulse periods (Schönherr *et al.* 1999). In some cell types, this phenomenon may be so pronounced as to stop cell firing: spike-frequency adaptation (Chiesa *et al.* 1997; Sacco *et al.* 2003). In our study the role of ERG channels in the spike-frequency adaptation has also been observed during the steady phase of step and ramp current injections, as shown by the longer decay time constant after ERG channel block. However, by examining the discharge responses of MVNn, during the dynamic phase of the current injections, it became apparent that ERG block caused a first spike latency shortening and a steeper rise time of firing. The effect on the first spike latency suggests that depolarizing commands are able to elicit, even early on, a sufficient amount of ERG current, which delays the first spike generation. The ERG current is further enhanced during the increasing current injection, by both membrane depolarization and higher neuronal activity and, this, in turn, slows down the firing progression. The amount of IF decay was variable and in some neurones it was not clearly detectable. Since these findings have particular implications for the processing of the synaptic inputs in the MVNn and the ERG channel may contribute to tune-up the appropriate filtering properties of the neurone, we tried to obtain more information on this issue by analysing neurone responses to sinusoidal current injections, at various frequencies. Indeed, we found that in many RNs, ERG channel block induces a significant gain enhancement of 20–30% and a phase lead of 10–30 deg in the range of 3–10 Hz and 1–10 Hz, respectively. This could indicate that ERG channels may influence the resonance properties of the neurones. However, not all

the RNs showed these gain and phase changes under ERG block, suggesting that the presence of the effect could be conditioned by other variables, such as the expression of different types of ERG channels, that might change the kinetics of the channel opening. We found, indeed, that in some neurones the amount of phase shift depended on the firing rate induced by the level of neuronal depolarization, suggesting that the basal firing activity of the neurone may affect the probability of ERG channel openings and inactivation. Therefore, it is possible that the phase shift could be no longer detectable if the imposed level of depolarization and firing rate is too high to somehow influence ERG channel contribution, negatively. As regards the type of neurones, it could also be conceivable that ERG channels might be distributed variously among the different types of MVNn and account for their distinct electrical properties. In our study, we distinguished type A from type B (Dutia & Johnston, 1998; Camp *et al.* 2006; Bagnall *et al.* 2007) and GABAergic from non-GABAergic neurones by using a recently proposed scheme based on peculiar electrophysiological properties (Bagnall *et al.* 2007). However, we did not find qualitative differences between type A and type B neurones, as well as between GABAergic and non-GABAergic neurones, upon ERG channel block, suggesting that the different types of MVNn express these channels. However, we cannot exclude possible quantitative differences, since we were only able to record a relatively small number of type A (GABAergic) neurones that therefore did not allow appropriate comparison.

In conclusion, we think that ERG channels contribute to setting the frequency and the discharge stability of vestibular neurones and to adapting their intrinsic properties to the signal processing. It may be suggested that ERG channels might play a critical role in mediating signal transformations from peripheral signals to the motor outputs, adapting the response in terms of amplitude and timing to the functional requirements particularly during high-frequency movements.

References

- Arcangeli A (2005). Expression and role of hERG channels in cancer cells. In *The Herp Cardiac Potassium Channel: Structure, Function and Long QT Syndrome*, Novartis Foundation Symposium, 266, ed. Chadwick DJ & Goode J, pp. 225–232. John Wiley & Sons Ltd, Chichester, UK.
- Babalian A, Vibert N, Assie G, Serafin M, Mühlethaler M & Vidal PP (1997). Central vestibular networks in the guinea-pig: functional characterization in the isolated whole brain *in vitro*. *Neuroscience* **81**, 405–426.
- Bagnall MW, Stevens RJ & du Lac S (2007). Transgenic mouse lines subdivide medial vestibular nucleus neurons into discrete, neurochemically distinct populations. *J Neurosci* **27**, 2318–2330.
- Bauer CK & Schwarz JR (2001). Physiology of EAG K⁺ channels. *J Membr Biol* **182**, 1–15.
- Camp AJ, Callister RJ & Brichta AM (2006). Inhibitory synaptic transmission differs in mouse type A and B medial vestibular nucleus neurons *in vitro*. *J Neurophysiol* **95**, 3208–3218.
- Canavier CC, Oprisan SA, Callaway JC, Ji H & Shepard PD (2007). Computational model predicts a role for ERG current in repolarizing plateau potentials in dopamine neurons: implications for modulation of neuronal activity. *J Neurophysiol* **98**, 3006–3022.
- Cherubini A, Taddei GL, Crociani O, Paglierani M, Buccoliero AM, Fontana L *et al.* (2000). HERG potassium channels are more frequently expressed in human endometrial cancer as compared to non-cancerous endometrium. *Br J Cancer* **83**, 1722–1729.
- Chiesa N, Rosati B, Arcangeli A, Olivotto M & Wanke E (1997). A novel role for HERG K⁺ channels: spike-frequency adaptation. *J Physiol* **501**, 313–318.
- de Waele C, Serafin A, Khateb M, Yabe T, Vidal PP & Mühlethaler M (1993). Medial vestibular nucleus in the guinea-pig: apamin-induced rhythmic burst firing, an *in vitro* and *in vivo* study. *Exp Brain Res* **95**, 213–222.
- du Lac S & Lisberger SG (1995). Membrane and firing properties of avian medial vestibular nucleus neurons *in vitro*. *J Comp Physiol* **176**, 641–651.
- Dutia MB & Johnston AR (1998). Development of action potentials and apamin-sensitive after-potentials in mouse vestibular nucleus neurones. *Exp Brain Res* **118**, 148–154.
- Dutia MB, Johnston AR & McQueen DS (1992). Tonic activity of rat medial vestibular nucleus neurones *in vitro* and its inhibition by GABA. *Exp Brain Res* **88**, 466–472.
- Faravelli L, Arcangeli A, Olivotto M & Wanke E (1996). A HERG-like K⁺ channel in rat F-11 DRG cell line: pharmacological identification and biophysical characterization. *J Physiol* **496**, 13–23.
- Furlan F, Taccola G, Grandolfo M, Guasti L, Arcangeli A, Nistri A & Ballerini L (2007). ERG conductance expression modulates the excitability of ventral horn GABAergic interneurons that control rhythmic oscillations in the developing mouse spinal cord. *J Neurosci* **27**, 919–928.
- Guasti L, Cilia E, Crociani O, Hofmann G, Polvani S, Becchetti A, Wanke E, Tempia F & Arcangeli A (2005). Expression pattern of the ether-a-go-go-related (ERG) family proteins in the adult mouse central nervous system: evidence for coassembly of different subunits. *J Comp Neurol* **491**, 157–174.
- Johnston AR, MacLeod NK & Dutia MB (1994). Ionic conductances contributing to spike repolarization and after-potentials in rat medial vestibular nucleus neurones. *J Physiol* **481**, 61–77.
- Lees-Miller JP, Kondo C, Wang L & Duff HJ (1997). Electrophysiological characterization of an alternatively processed ERG K⁺ channel in mouse and human hearts. *Circ Res* **81**, 719–726.
- Lin Y & Carpenter DO (1993). Medial vestibular neurons are endogenous pacemakers whose discharge is modulated by neurotransmitters. *Cell Mol Neurobiol* **13**, 601–613.

- London B, Trudeau MC, Newton KP, Beyer AK, Copeland NG, Gilbert DJ, Jenkins NA, Satler CA & Robertson GA (1997). Two isoforms of the mouse ether-a-go-go-related gene coassemble to form channels with properties similar to the rapidly activating component of the cardiac delayed rectifier K^+ current. *Circ Res* **81**, 870–878.
- Masi A, Becchetti A, Restano-Cassulini R, Polvani S, Hofmann G, Buccoliero AM *et al.* (2005). hERG1 channels are overexpressed in glioblastoma multiforme and modulate VEGF secretion in glioblastoma cell lines. *Br J Cancer* **93**, 781–792.
- Nedergaard S (2004). A Ca^{2+} -independent slow afterhyperpolarization in substantia nigra compacta neurons. *Neuroscience* **125**, 841–852.
- Papa M, Boscia F, Canitano A, Castaldo P, Sellitti S, Annunziato L & Taglialatela M (2003). Expression pattern of the ether-a-go-go-related (ERG) K^+ channel-encoding genes ERG1, ERG2, and ERG3 in the adult rat central nervous system. *J Comp Neurol* **466**, 119–135.
- Polvani S, Masi A, Pillozzi S, Gragnani L, Crociani O, Olivotto M, Becchetti A, Wanke E & Arcangeli A (2003). Developmentally regulated expression of the mouse homologues of the potassium channel encoding genes m-erg1, m-erg2 and m-erg3. *Gene Expr Patterns* **3**, 767–776.
- Sacco T, Bruno A, Wanke E & Tempia F (2003). Functional roles of an ERG current isolated in cerebellar Purkinje neurons. *J Neurophysiol* **90**, 1817–1828.
- Saganich MJ, Machado E & Rudy B (2001). Differential expression of genes encoding subthreshold-operating voltage-gated K^+ channels in brain. *J Neurosci* **21**, 4609–4624.
- Sanguinetti MC & Jurkiewicz NK (1990). Two components of cardiac delayed rectifier K^+ current. Differential sensitivity to block by class III antiarrhythmic agents. *J Gen Physiol* **96**, 195–215.
- Schönherr R, Rosati B, Hehl S, Rao VG, Arcangeli A, Olivotto M, Heinemann SH & Wanke E (1999). Functional role of the slow activation property of ERG K^+ channels. *Eur J Neurosci* **11**, 753–760.
- Schwarz JR & Bauer CK (2004). Functions of erg K^+ channels in excitable cells. *J Cell Mol Med* **8**, 22–30.
- Serafin M, de Waele C, Khateb A, Vidal PP & Mühlethaler M (1991a). Medial vestibular nucleus in the guinea-pig. I. Intrinsic membrane properties in brainstem slices. *Exp Brain Res* **84**, 417–425.
- Serafin M, de Waele C, Khateb A, Vidal PP & Mühlethaler M (1991b). Medial vestibular nucleus in the guinea-pig. II. Ionic basis of the intrinsic membrane properties in brainstem slices. *Exp Brain Res* **84**, 426–433.
- Shi W, Wymore RS, Wang HS, Pan Z, Cohen IS, McKinnon D & Dixon JE (1997). Identification of two nervous system-specific members of the erg potassium channel gene family. *J Neurosci* **17**, 9423–9432.
- Smith MR, Nelson AB & du Lac S (2002). Regulation of firing response gain by calcium-dependent mechanisms in vestibular nucleus neurons. *J Neurophysiol* **87**, 2031–2042.
- Spinelli W, Moubarak IF, Parsons RW & Colatsky TJ (1993). Cellular electrophysiology of WAY-123,398, a new class III antiarrhythmic agent: specificity of IK block and lack of reverse use dependence in cat ventricular myocytes. *Cardiovasc Res* **27**, 1580–1591.
- Straka H, Vibert N, Vidal PP, Moore LE & Dutia MB (2005). Intrinsic membrane properties of vertebrate vestibular neurons: function, development and plasticity. *Prog Neurobiol* **76**, 349–392.
- Takazawa T, Saito Y, Tsuzuki K & Ozawa S (2004). Membrane and firing properties of glutamatergic and GABAergic neurons in the rat medial vestibular nucleus. *J Neurophysiol* **92**, 3106–3120.
- Warmke JW & Ganetzky B (1994). A family of potassium channel genes related to erg in *Drosophila* and mammals. *Proc Natl Acad Sci U S A* **91**, 3438–3442.

Acknowledgements

The financial support of Telethon-Italy (Grant GGP030159), MIUR-COFIN 2005, COMPAGNIA di San Paolo (Turin) and Fondazione Cassa di Risparmio di Perugia to M.P., and MIUR-PRIN 2006 and Ente Cassa di Risparmio di Firenze to A.A. is gratefully acknowledged. We thank Olivia Crociani, Adele Frondaroli and Fabio Botti for their contributions, Hilary A. Giles for English editing, and Domenico Bambagioni and Ezio Mezzasoma for outstanding technical assistance.

Supplemental material

Online supplemental material for this paper can be accessed at: <http://jp.physoc.org/cgi/content/full/jphysiol.2008.155762/DC1>